REPORT DOCUMENTATION PAGE

Form Approved OMB NO. 0704-0188

1. REPORT DATE (DD-MM-YYYY)	2. REPORT TYPE	3. DATES COVERED (From - To)
	Old Reprint	-

4. TITLE AND SUBTITLE

Maximum-likelihood estimation forfrequency-modulated continuous-wave laser rangingusing photon-counting detectors

5a. CONTRACT NUMBER	W911NF-11-1-0540
5b. GRANT NUMBER	
5c. PROGRAM ELEMENT NUMBER	1D10BQ
5d. PROJECT NUMBER	
5e. TASK NUMBER	
5f. WORK UNIT NUMBER	

6. AUTHORS

Baris I Erkmen, Zeb W Barber, Jason R Dahl

7. PERFORMING ORGANIZATION NAMES AND ADDRESSES

Montana State University
Civil Engineering
Montana State University
Bozeman, MT 59717 -2470

8. PERFORMING ORGANIZATION REPORT NUMBER

9. SPONSORING/MONITORING AGENCY NAME(S) AND ADDRESS(ES)

U.S. Army Research Office
P.O. Box 12211
Research Triangle Park, NC 27709-2211

10. SPONSOR/MONITOR'S ACRONYM(S)
ARO

11. SPONSOR/MONITOR'S REPORT NUMBER(S)
61101-PH-DRP.1

12. DISTRIBUTION AVAILIBILITY STATEMENT

Approved for public release; distribution is unlimited.

13. SUPPLEMENTARY NOTES

The views, opinions and/or findings contained in this report are those of the author(s) and should not contrued as an official Department of the Army position, policy or decision, unless so designated by other documentation.

14. ABSTRACT

We analyze the minimum achievable mean-square error in frequencymodulated continuous-wave (FMCW) range estimation of a single stationary target when photon counting detectors are employed. Starting from the probability density function for the photon arrival times, we derive the Cram´er-Rao bound (CRB) and highlight three important regimes: the

15. SUBJECT TERMS

laser ranging, frequency estimation, photon counting

16. SECURITY CLASSIFICATION OF:			17. LIMITATION OF ABSTRACT	15. NUMBER OF PAGES	19a. NAME OF RESPONSIBLE PERSON
a. REPORT	b. ABSTRACT	c. THIS PAGE			Zeb Barber
UU	UU	UU	UU		19b. TELEPHONE NUMBER: 406-994-5925

Report Title

Maximum-likelihood estimation forfrequency-modulated continuous-wave laser rangingusing photon-counting detectors

ABSTRACT

We analyze the minimum achievable mean-square error in frequencymodulated continuous-wave (FMCW) range estimation of a single stationary target when photon counting detectors are employed. Starting from the probability density function for the photon arrival times, we derive the Cram´er-Rao bound (CRB) and highlight three important regimes: the dark-noise-dominated regime wherein the CRB improves quadratically with the mean received photon number, the shot-noise-dominated regime (i.e., the standard quantum limit) in which the improvement is linear, and the dead-time-dominated regime wherein the CRB is constant. We show that if both signal and reference photons cost equal, the shot-noise-limited CRB is minimized when the local field strength is equal to that of the target-return field, and the average frequency-modulation energy determines the performance. Simulation of the maximum-likelihood (ML) estimator shows that its performance approaches the standard quantum limit only when the mean received photons are between two thresholds. We provide analytic approximations to these thresholds for linear frequency modulation. Finally, we report on a proof-of-concept experiment in which ML estimation outperforms conventional beat-frequency estimation.

REPORT DOCUMENTATION PAGE (SF298)
(Continuation Sheet)

Continuation for Block 13

ARO Report Number 61101.1-PH-DRP
Maximum-likelihood estimation forfrequency-mo ...

Block 13: Supplementary Note

Approved for public release; distribution is unlimited.

Maximum-likelihood estimation for frequency-modulated continuous-wave laser ranging using photon-counting detectors

Baris I. Erkmen[1], Zeb W. Barber[2], Jason R. Dahl[2]

[1,*] *Jet Propulsion Laboratory, California Institute of Technology, 4800 Oak Grove Drive, Pasadena, CA 91109, USA.*

[2] *Spectrum Lab, Montana State University, Bozeman, MO 59717, USA.*

[*] *Corresponding author: baris.i.erkmen@jpl.nasa.gov*

We analyze the minimum achievable mean-square error in frequency-modulated continuous-wave (FMCW) range estimation of a single stationary target when photon counting detectors are employed. Starting from the probability density function for the photon arrival times, we derive the Cramér-Rao bound (CRB) and highlight three important regimes: the dark-noise-dominated regime wherein the CRB improves quadratically with the mean received photon number, the shot-noise-dominated regime (i.e., the standard quantum limit) in which the improvement is linear, and the dead-time-dominated regime wherein the CRB is constant. We show that if both signal and reference photons cost equal, the shot-noise-limited CRB is minimized when the local field strength is equal to that of the target-return field, and the average frequency-modulation energy determines the performance. Simulation of the maximum-likelihood (ML) estimator shows that its performance approaches the standard quantum limit only when the mean received photons are between two thresholds. We provide analytic approximations to these thresholds for linear frequency modulation. Finally, we report on a proof-of-concept experiment in which ML estimation outperforms conventional beat-frequency estimation.

OCIS codes: 010.3640, 270.5290, 030.5260, 000.5490, 040.1345

1. Introduction

In its essence, optical ranging is a problem of estimating the round-trip flight time of a phase- or amplitude-modulated optical beam that reflects off of a target. Frequency modulated continuous-wave (FMCW) ranging systems obtain this estimate by performing an interferometric measurement between a local frequency-modulated laser beam and a delayed copy returning from the target. The range estimate is formed by mixing the target-return field

with the local reference field on a beamsplitter and detecting the resultant beat modulation. In conventional FMCW ranging the source modulation is linear in instantaneous frequency, the reference-arm field has many more photons than the target-return field, and the time-of-flight estimate is generated by balanced difference-detection of the beamsplitter output, followed by a frequency-domain peak search. This technique is well-known to achieve range resolution proportional to $c/2\Delta f$ in a T-second chirp window, where c is the speed-of-light, Δf is the chirp bandwidth, and the time-bandwidth product satisfies $T\Delta f \gg 1$ [1, 2].

Important advances have been reported in the recent literature for FMCW ranging systems. To revisit several examples, very broad chirp bandwidths have been achieved using active feedback stabilization [3, 4]. Alternative frequency modulation functions, such as sinusoidal modulation [5, 6] and pseudorandom modulation [7], have been employed to improve the range resolution. These results, and much of the literature in general, has focused on the strong-local-oscillator regime, wherein the mean photon number in the reference field greatly exceeds that in the target-return field over the integration window of interest. This limitation has been removed in recent work [8], where target detection with a weak local oscillator has been analyzed in detail.

Although the literature on improving the performance of FMCW ranging systems is extensive, limited results are available on its ultimate performance bounds, which is governed—after all technical noises have been eliminated—by the photodetection statistics resulting from the quantum nature of the incident optical fields. With high efficiency, high bandwidth, and low noise photon-counting detector technologies rapidly maturing, it is feasible to anticipate that FMCW ranging systems will utilize photon-counting detectors in the near future. Therefore, in this paper we focus both on determining the ultimate estimation accuracy afforded by FMCW ranging, and on estimation algorithms that approach this performance. Because range is related to time delay by a constant (the speed of light), we present all of our results in terms of the latter and omit the trivial scaling of these results to express them as range. Our treatment is founded on a rigorous statistical characterization of the

(random) photoelectron emission times as a function of the incident optical field, including the deleterious effects caused by dark current and dead time. These statistics permit us to derive the Cramér-Rao lower bound (CRB) on the accuracy of FMCW ranging and to derive the maximum-likelihood (ML) estimator, whose performance approaches this bound under some photon-flux conditions. Here, we determine these conditions and validate the theory via simulation and experiment. Because our emphasis is on FMCW receivers employing photon-counting detectors, we limit the focus of this paper to analyzing the performance when a single specularly-reflecting target is present within the range of interest. Nonetheless, the formalism developed herein could be extended to include diffuse target reflections [9], multiple targets within the range-of-interest [10], and atmosphere-induced distortions [11], with the appropriate modifications to statistics governing the output processes of the photon-counting detectors.

Our paper is organized as follows. In Section 2 we define the problem of interest, and then we derive the CRB for arbitrary frequency modulation. First, we consider only the shot noise of the incident (coherent-state) fields, and determine the optimal strength of the local reference field relative to that of the target-return, as well as the CRBs achieved by different modulation functions. We then extend our formalism to include dark counts and dead time in the detector, and quantify the degradation in performance. In Section 3, we derive the ML estimator and show via simulation that when the total mean received photon number is between two thresholds its mean-square error approaches the CRB. We derive analytic approximations to these threshold values for the case of linear frequency modulation. Finally, in Section 4, we report experiments with linear frequency modulation and show that the ML estimator performs better than the conventional difference-detection followed by frequency-domain estimation of the beat frequency. Section 5 concludes the paper with a discussion of our key results.

2. Problem formulation and the Cramér-Rao bound

Figure 1 illustrates the FMCW ranging system in consideration. We assume that an ideal laser field[1] with center frequency ω_c is split via a beamsplitter into a signal field $E_{S,1}(t)e^{-i\omega_c t}$ and a reference field $E_{R,1}(t)e^{-i\omega_c t}$, where $E_{k,1}(t) = \sqrt{N_{k,1}/T}e^{i\phi(t)}$ for $0 < t \leq T$ and $k = S, R$ denotes their complex baseband temporal modulations. Here, $E_{k,1}(t)$ are normalized to have units $\sqrt{\text{photons/s}}$, such that $N_{k,1}$ denotes the mean photon number over the T-second window. The signal field is transmitted to interact with the target, yielding a target-return field $E_{S,2}(t)$. In this paper we have assumed a single specularly-reflecting target, so $E_{S,2}(t) = r_S E_{S,1}(t - t_0)$, where $r_S \leq 1$ is the field reflection coefficient and $t_0 \in \mathcal{T}$ is the relative time delay between the signal- and reference-arm fields within the *a priori* domain of uncertainty $\mathcal{T}$. The reference arm field remains local to the ranging instrument, and is therefore assumed to go through a simple attenuation by $r_R \leq 1$, yielding $E_{R,2}(t) = r_R E_{R,1}(t)$. The receiver mixes the target-return field and the reference field with a 50/50 beam-splitter, resulting in

$$E_{D,m}(t) = \frac{E_{S,2}(t) + (-1)^{m+1}E_{R,2}(t)}{\sqrt{2}}, \tag{1}$$

at its two output ports $m = 1, 2$. $E_{D,m}(t)$ are incident on two matched photon counters for $t \in (0, T]$, giving rise to the photocurrent processes $i_m(t)$. We assume $i_m(t)$ are normalized by the electron charge to have units photoelectrons/s, and are therefore sequences of unit-area impulses occurring at each photoelectron emission epoch.[2] With ideal laser light incident on the photodetectors, $i_m(t)$ are independent discrete stochastic point processes whose statistics are governed by several uncertainties. First, energy measurements on coherent-state fields are stochastic due to the quantum nature of light (shot noise) [13]. Second, there are stochastic

[1] Throughout this paper an *ideal laser field* refers to a paraxial and quasimonochromatic optical field in a single spatial and polarization mode, which is also in a coherent state of the quantized field operator, such that it gives rise to Poisson statistics when an ideal photon-counting measurement is performed on it [12].

[2] This characterization of the photodetector output implies that the detector has infinite electrical bandwidth, allowing the arrival times to be precisely resolvable. In practice, there is little loss in adopting this idealization if the photodetector impulse response is significantly narrower than the mean photoelectron interarrival time.

electron emissions from the photosensitive area of the detector when no light is incident (dark counts). Third, after every photoelectron emission there is a period during which the detector is unable to generate any additional photoelectrons regardless of the incident field amplitude (dead time). The first of these effects is fundamental, whereas the latter two are practical limitations to state-of-the-art photon counters that can be improved upon in the future.

An important component in the Fig. 1 system is the algorithm that generates an estimate $\hat{t}_0$ of the time delay t_0, based on the occurrence times of the photoelectrons from the two detectors. Different estimators will achieve different mean-square error values, an exhaustive characterization of which is not feasible. The CRB, on the other hand, is a lower bound on the mean-square error achievable by any unbiased estimator [2]. Furthermore, the CRB is achieved by the ML estimator *if* an efficient estimator exists, and even if one does not exist the ML estimator often asymptotically approaches the CRB at high signal flux. Therefore, we first derive the CRB for the FMCW ranging system described above. Then, we focus on the ML estimator and evaluate its performance relative to the CRB.

2.A. The standard quantum limit

Let us first consider near-ideal photon counters and develop some insights into the ultimate performance of FMCW ranging. When $E_{D,1}(t)$ and $E_{D,2}(t)$ are incident on matched photon-counting detectors with quantum efficiency η, zero dark current and zero dead time, $i_m(t)$ are statistically independent inhomogeneous Poisson point processes with rate functions [14]

$$\Lambda_m(t;t_0) = \frac{\eta N_I}{2T}\Big[1 + (-1)^{m+1}\beta\cos\big(D(t;t_0)\big)\Big], \tag{2}$$

for $m = 1, 2$.[3] Here, $D(t; t_0) \equiv \phi(t) - \phi(t - t_0)$ is the beat modulation that carries information on t_0,

$$\beta \equiv \frac{2\sqrt{N_{S,2} N_{R,2}}}{N_{S,2} + N_{R,2}} \tag{3}$$

is a parameter between 0 and 1 indicating the relative strength of the target-return and reference fields in terms of their mean photon numbers $N_{k,2} \equiv r_k^2 N_{k,1}$ for $k = S, R$, and $N_I \equiv N_{S,2} + N_{R,2}$ is the total mean number of photons incident on the two detectors. The probability density function for observing n_1 photodetection events in the first detector at event times $\{u_1, \ldots, u_{n_1}\} \in [0, T]$ and n_2 photodetection events in the second detector at event times $\{v_1, \ldots, v_{n_2}\} \in [0, T]$, is given by [14]

$$\begin{aligned} &p(n_1, u_1, \ldots, u_{n_1}, n_2, v_1, \ldots, v_{n_2}; t_0) \\ &\qquad = \left[\prod_{i=1}^{n_1} \Lambda_1(u_i; t_0)\right] \left[\prod_{j=1}^{n_2} \Lambda_2(v_j; t_0)\right] e^{-\int_0^T \mathrm{d}t \, [\Lambda_1(t;t_0) + \Lambda_2(t;t_0)]}. \end{aligned} \tag{4}$$

From Eq. (4), the CRB for t_0 is expressed as [2]

$$\mathrm{CRB} \equiv -\left\langle \frac{\partial^2 \log p(n_1, u_1, \ldots, u_{n_1}, n_2, v_1, \ldots, v_{n_2}; t_0)}{\partial t_0^2} \right\rangle^{-1}, \tag{5}$$

where the angled brackets denote the expectation over all of the random variables.

In the Appendix we show that substituting Eqs. (2) and (4) into (5) leads to

$$\mathrm{CRB} = \frac{1}{\eta N_I} \left[\frac{1}{T} \int_0^T \mathrm{d}t \, \frac{\beta^2 \sin^2\big(D(t; t_0)\big)}{1 - \beta^2 \cos^2\big(D(t; t_0)\big)} \dot{\phi}^2(t - t_0)\right]^{-1}, \tag{6}$$

where $\dot{\phi}(t) \equiv \mathrm{d}\phi(t)/\mathrm{d}t$. For a fixed ratio between the target-return and the reference-arm mean photon numbers, i.e., for β constant, the CRB follows a $1/N_I$ scaling, which is referred to as the *standard quantum limit* because it is the best possible scaling achievable with

[3] We use the common notation that the variable t in the argument of the rate function is separated from the parameter of interest t_0 with a semi-colon.

photon counting of ideal laser fields. In addition, because the first term in the integrand is maximized at $\beta = 1$ for all t, we find

$$\mathrm{CRB} \geq \frac{1}{\eta N_I} \left[\frac{1}{T} \int_0^T \mathrm{d}t \, \dot{\phi}^2(t) \right]^{-1}, \tag{7}$$

for all $N_I \geq 0$ and $t_0 \in \mathcal{T}$, with equality if and only if $\beta = 1$. This optimal CRB is the main result of this section, and it leads to several important insights. First, given a total mean received photon number N_I it is optimal to have $N_{S,2} = N_{R,2}$. Second, whereas in general the CRB depends on t_0, the optimal CRB is independent of the true value of the parameter to be estimated. Finally, the optimal CRB depends only on the average energy ($\mathcal{L}_2$ norm) of the frequency modulation function. Therefore, all frequency modulations with equal $\mathcal{L}_2$ norm attain the same optimized CRB. Table 1 summarizes the $\mathcal{L}_2$ norms of several commonly employed frequency modulations in FMCW ranging, quantifying their relative performance at equal N_I.

Setting $\beta \ll 1$ in Eq. (6), we derive the CRB in the strong reference-arm regime as

$$\mathrm{CRB} \approx \frac{1}{\beta^2 \eta N_I} \left[\frac{1}{T} \int_0^T \mathrm{d}t \, \sin^2\big(D(t;t_0)\big) \dot{\phi}^2(t - t_0) \right]^{-1}, \tag{8}$$

where the term outside the brackets is approximately equal to $1/(4\eta N_{S,2})$. This CRB is significantly worse than the optimal CRB derived above. This is because we have assessed equal cost to *both* signal photons and reference photons in deriving the optimal CRB. This cost assignment pertains to scenarios where local resources and those used for target interaction are optimized jointly, e.g., to minimize wall-plug power consumption. However, alternative cost assignments are also possible. For example, in noninvasive imaging of a biological sample or to ensure low probability of detection in a military application, it may be more appropriate to assign cost only to the photons that interrogate the target and have cost-free reference-arm photons. It is straightforward to optimize—possibly numerically—the Eq. (6) expression for various cost assignments in the two arms, but here for brevity we restrict our attention to

the equal-cost scenario.

In Fig. 2 we have plotted the ratio of the CRB from Eq. (6) to the optimal CRB in Eq. (7), as a function of $\beta \in (0, 1]$. The slope of this ratio is steep for $\beta \approx 1$, which causes significant penalty for a small deviation from the optimum. As β decreases from 1 towards 0 the ratio eventually becomes proportional to $1/\beta^2$ and converges to the strong-reference-arm approximation above. We observe from the figure that this convergence occurs when $\beta < 0.3$.

2.B. Dark noise and dead time

The results above define the best possible performance attainable with ideal laser light and near-ideal photon counting, with subunity quantum efficiency being the only nonideal effect. Now we add dark counts and dead time to quantify the degradation in the CRB relative to the standard quantum limit.

Suppose that the photon-counting detectors from Fig. 1 have equal and constant dark count rates λ_d, but no dead time. Then, the dark counts in each detector form a homogeneous Poisson process with statistics equivalent to having on average $N_d \equiv \lambda_d T/\eta$ additional photons incident in a T-second interval. Therefore, the two photodetector outputs are independent inhomogeneous Poisson processes as stated in the previous subsection, but now with the modified rate functions

$$\Lambda_{m,d}(t; t_0) = \frac{\eta N_{I,d}}{2T}\Big[1 + (-1)^{m+1}\beta_d \cos\big(D(t; t_0)\big)\Big] \tag{9}$$

for $m = 1, 2$, where $N_{I,d} \equiv N_I + 2N_d$ and $\beta_d \equiv \beta/(1 + 2N_d/N_I)$ are the two parameters that are modified due to dark counts. Next, suppose that the detectors also have equal and deterministic nonparalyzing dead time τ.[4] In this case, the rate function itself becomes a stochastic process that causally depends on prior arrival times. Consequently, the detector output is modeled as a *self-exciting* point process [14]. The probability density function for

[4] A nonparalyzable photon counter is one in which a photon absorption or a spontaneous charge release during a dead time does not extend the duration of the dead time interval. Dead time may be random in general, but for analytic simplicity here we assume it is a deterministic period.

observing n_1 photodetection events in the first detector at event times $\{u_1, \ldots, u_{n_1}\} \in [0, T]$ and n_2 photodetection events in the second detector at event times $\{v_1, \ldots, v_{n_2}\} \in [0, T]$ is now given by [14]

$$p(n_1, u_1, \ldots, u_{n_1}, n_2, v_1, \ldots, v_{n_2}; t_0) = p_d(n_1, u_1, \ldots, u_{n_1}; t_0) p_d(n_2, v_1, \ldots, v_{n_2}; t_0), \tag{10}$$

where

$$\begin{aligned} p_d(n_m, u_1, \ldots, u_{n_m}) \equiv & \left[\prod_{i=1}^{n_m} \Lambda_{m,d}(u_i; t_0) \right] \\ & \times \exp\left\{ - \int_0^{u_1} \mathrm{d}t \, \Lambda_{m,d}(t; t_0) - \sum_{i=2}^{n_m+1} \int_{u_{i-1}}^{u_i} \mathrm{d}t \, \Lambda_{m,d}(t; t_0) w_\tau(t - u_{i-1}) \right\} \end{aligned} \tag{11}$$

for $m = 1, 2$. Here, we have defined $u_{n_m+1} \equiv T$ for compactness of the expression, and $w_\tau(t) \equiv 1$ if $t > \tau$ but is 0 otherwise.

Deriving the CRB is straightforward by substituting Eqs. (10) and (11) into Eq. (5), so we postpone the tedious details to the Appendix. Here we highlight several asymptotes to the CRB expression when the rate of change of $\Lambda_{m,d}(t; t_0)$ is much slower than $1/\tau$, specifically, when the frequency modulation and dead time satisfy $|\dot{\phi}(t) - \dot{\phi}(t - t_0)|\tau \ll 1$ for all $t \in (0, T]$ and $t_0 \in \mathcal{T}$:

$$\mathrm{CRB} \approx \begin{cases} \frac{2N_d(1+\alpha)}{\eta N_I^2 \beta^2} K_1^{-1}(t_0) & N_I \ll 2N_d \text{ and } \alpha \ll 1 \\ \frac{1}{\eta N_I} K_2^{-1}(\beta, t_0) & N_I \gg 2N_d \text{ and } \alpha \ll 1 \\ \frac{\tau}{2T} K_3^{-1}(\beta, t_0) & N_I \gg 2N_d \text{ and } \alpha \gg 1, \end{cases} \tag{12}$$

where $\alpha \equiv \eta N_{I,d} \tau / (2T)$ is the average fraction of photoelectron counts lost during the dead

times, and the three terms independent of photon number are

$$K_1(t_0) = \frac{1}{T}\int_0^T \mathrm{d}t\, \sin^2\big(D(t;t_0)\big)\dot{\phi}^2(t-t_0), \tag{13}$$

$$K_2(\beta,t_0) = \frac{1}{T}\int_0^T \mathrm{d}t\, \frac{\beta^2\sin^2\big(D(t;t_0)\big)}{1-\beta^2\cos^2\big(D(t;t_0)\big)}\dot{\phi}^2(t-t_0), \text{ and} \tag{14}$$

$$K_3(\beta,t_0) = \frac{1}{T}\int_0^T \mathrm{d}t\, \frac{\beta^2\sin^2\big(D(t;t_0)\big)\big[1+\beta^2\cos^2\big(D(t;t_0)\big)\big]}{\big[1-\beta^2\cos^2\big(D(t;t_0)\big)\big]^2}\dot{\phi}^2(t-t_0). \tag{15}$$

The asymptotic expressions in Eq. (12) represent three distinct trends with respect to the mean incident photon number. When the mean dark count is significantly greater than the mean signal photon count ($N_d \gg N_I$) and dead time is short enough to have negligible impact on the arrival rate ($\alpha \ll 1$), the performance is *dark-noise dominated*. In this regime the CRB is significantly worse than the standard quantum limit, and it improves quadratically as the mean incident photon number increases. At the other extreme, when the mean incident photon number is so large that the detector is almost universally blocked by dead time ($\alpha \gg 1$) the output of the photon-counting detectors saturate irrespective of the mean received photon number. Here the performance is *dead-time dominated* and the CRB reaches a floor. Often there is an intermediate regime between these two extremes wherein the signal counts dominate over dark counts ($N_I \gg N_d$), yet the dead time impact is negligible ($\alpha \ll 1$). In this regime the performance is *shot-noise dominated* and the CRB approaches the standard quantum limit. If dark counts or dead time are too high, the ranging performance may never become shot-noise dominated, thus the standard quantum limit may not be attainable.

In Fig. 3 we have plotted the CRB, normalized by T^2 to render it dimensionless, when $\dot{\phi}(t) = \Delta f t/T$, i.e., when linear frequency modulation is employed. The dashed curves correspond to the aforementioned asymptotes, and the solid line is the numerically-evaluated CRB from Eq. (42) in the Appendix. The figure indicates that the asymptotes provide a good approximation to the CRB in their applicable regime. Furthermore, the transition thresholds are well-approximated by the intersection points of these asymptotes.

3. Maximum-likelihood estimation of range

In this section we derive the ML estimator and show via simulation that its performance approaches the CRB when the incident photon number satisfies $N_\ell < N_I < N_u$, where N_ℓ and N_u are lower and upper breakdown thresholds respectively. The lower threshold is due to t_0 having a nonlinear relation to the observation statistics, whereas the upper threshold is due to dead time dominating the observation statistics. We will derive analytic approximations for N_ℓ and N_u in the case of linear frequency modulation.

The ML estimator is defined as

$$\hat{t}_0 \equiv \arg\max_{t_0 \in \mathcal{T}} \log p(n_1, u_1, \ldots, u_{n_1}, n_2, v_1, \ldots, v_{n_2}; t_0), \tag{16}$$

where $\mathcal{T}$ is the support of t_0. Using the probability density function in Eq. (10) and following straightforward simplifications (see the Appendix for details omitted here) we arrive at

$$\hat{t}_0 = \arg\max_{t_0 \in \mathcal{T}} \int_0^T \mathrm{d}t \left[i_1(t) h_1(t; t_0) + i_2(t) h_2(t; t_0) \right], \tag{17}$$

where the impulse responses are given by

$$h_m(t; t_0) = \log\Big(1 + (-1)^{m+1} \beta_d \cos\big(D(t; t_0)\big)\Big) + (-1)^{m+1} \alpha \beta_d \cos\big(D(t; t_0)\big), \tag{18}$$

for $m = 1, 2$. Thus, a sufficient statistic for the ML estimator is the sum of filtered photodetector outputs, where the filter impulse responses are linear and time-varying.

Let us consider several limiting cases of this general estimator. When dead time is negligible, i.e. $\alpha \ll 1$, only the first term in Eq. (18) survives, and the impulse responses

$$h_m(t; t_0) \equiv \log\Big(1 + (-1)^{m+1} \beta_d \cos\big(D(t; t_0)\big)\Big) \tag{19}$$

are recognizable as the log-matched filters to the photoelectron generation rates in each

detector. If $\beta_d \ll 1$ and α is arbitrary, which occurs with a strong local field ($\beta \ll 1$) or when dark noise dominates the signal energy ($N_d \gg N_I$), the ML estimator can be simplified as

$$\hat{t}_0 \approx \arg\max_{t_0 \in \mathcal{T}} \int_0^T \mathrm{d}t \, \big(i_1(t) - i_2(t)\big) \cos\big(D(t; t_0)\big), \tag{20}$$

i.e., difference detection followed by a matched filter to the rate function generates a sufficient statistic. If we further specialize our result to linear frequency modulation $\dot{\phi}(t) = \Delta f t/T$, we obtain

$$\hat{t}_0 \approx \arg\max_{t_0 \in \mathcal{T}} \Re\Big\{ e^{i\Delta f t_0^2/(2T)} \int_0^T \mathrm{d}u \, \big(i_1(u) - i_2(u)\big) e^{-i\Delta f t_0 u/T} \Big\}, \tag{21}$$

i.e., difference detection followed by a Fourier transform and peak detection, which is often used in practice as the range estimator, is also approximately the ML estimator in this regime. This result is not surprising. Having a strong local field or having noise dominated by dark counts both imply that the photodetector output processes have a signal-dependent mean, but a largely signal-independent noise process. This, together with a Gaussian random process approximation that becomes asymptotically tight when the photoelectron counts are large, yields an additive Gaussian noise channel for which the aforementioned estimator is exactly maximum-likelihood achieving [2].

Figures 4–5 plot the simulated mean-square error (MSE) of the ML estimator for linear frequency modulation as a function of ηN_I. Figure 4 represents the near-optimal case with $N_d = 0$ and $\tau = 0$ and $\beta \approx 1$. We observe that the ML estimator tracks the CRB well for large values of N_I. However, when N_I falls below a threshold, which we denote with N_ℓ, the estimator performance rapidly deteriorates towards a uniformly-distributed random guess of $t_0 \in \mathcal{T}$. Figure 5(a) includes dark counts and dead time, specifically $N_d = 1$ and $\tau = 100\,\mathrm{ns}$, and Fig. 5(b) shows a case when $\beta \ll 1$. In both cases, the qualitative behavior is the same. First, as in the case with no dark counts and dead time, for $N_I < N_\ell$ the estimator rapidly deteriorates to random uniform guesses. However, unlike the previous case, a second breakdown regime is observed when N_I exceeds a threshold we denote as N_u. In all three

cases the MSE performance is consistent with the CRB for some region of N_I, but otherwise deviates from this optimal bound. It is important to determine this region in terms of the relevant system parameters, so that the CRB is utilized for performance predictions only within this N_I regime.

3.A. The lower breakdown threshold N_ℓ

We will restrict our derivation to the case of linear frequency modulation. Our approach—motivated by prior literature—will be to first introduce an analytic model that approximates the MSE of the ML estimator, and then to derive N_ℓ from this model [15–17].

State-of-the art photon counting detectors yield typically better than kHz-rate dark counts, which implies no more than low tens of dark counts per realistic integration windows ($\sim$ 1–10 msec). Because we observe that the threshold often occurs at much greater photon numbers, we assume $N_d \approx 0$ in subsequent derivation. We also assume that N_ℓ occurs in a regime where the photon flux is low enough to warrant the $\alpha \approx 0$ approximation. We begin by assuming that all possible outcomes can be grouped into two classes of events: 1) *typical* events, i.e., those outcomes that are sufficiently informative and yield average performance close to the CRB, and 2) *atypical* events, i.e., those outcomes that give little to no information and yield average performance close to a random uniform guess of $t_0 \in \mathcal{T}$.[5] Based on this classification we write the MSE model for the ML estimator as

$$\left\langle (t_0 - \hat{t}_0)^2 \right\rangle = \sigma_{\mathcal{A}}^2 P_{\mathcal{A}} + \mathrm{CRB}(1 - P_{\mathcal{A}}), \tag{22}$$

where the CRB is given by Eq. (42), but with $N_d = 0$ and $\alpha = 0$ it simplifies to the Eq. (6) expression. $P_{\mathcal{A}}$ denotes the probability that the observed photon arrival sequence belongs to the atypical set, and

$$\sigma_{\mathcal{A}}^2 \equiv \frac{(T_2 - T_1)^2}{12} + \left(\frac{T_2 + T_1}{2} - t_0 \right)^2 \tag{23}$$

[5] We have implicitly assumed that the estimator is required to generate an estimate at the end of the observation period, regardless of the event outcome.

is the MSE of a uniform random guess. Here we have used $T_1 \equiv \min_{t_0 \in \mathcal{T}} t_0$ and $T_2 \equiv \max_{t_0 \in \mathcal{T}} t_0$ to denote the end-points of $\mathcal{T}$. From the Eq. (22) model we define N_ℓ as the N_I value that satisfies

$$P_{\mathcal{A}} \sigma_{\mathcal{A}}^2 = (1 - P_{\mathcal{A}}) \mathrm{CRB}. \tag{24}$$

Thus, good agreement between the model and the simulated performance hinges on an accurate characterization of $P_{\mathcal{A}}$. When the total photoelectron count is zero or one, the ML estimate is uniform over $\mathcal{T}$, corresponding to atypical events. So, we can write

$$P_{\mathcal{A}} = P(n < 2) + P(n \geq 2) P_{\mathcal{A}|2} \tag{25}$$

where $n \equiv n_1 + n_2$ is the total number of counts from both detectors within the observation window, $P(n < 2) = (1 + \eta N_I) e^{-\eta N_I}$, and $P_{\mathcal{A}|2}$ denotes the atypical event probability conditioned on two or more arrivals. Unfortunately, it is impractical to ascertain the precise subset of outcomes that are atypical. Therefore, we resort to deriving a tractable approximation to $P_{\mathcal{A}|2}$ in the $\beta \ll 1$ and $N_I \gg 1$ limit, then using it universally.

To evaluate $P_{\mathcal{A}|2}$, recall from Eq. (21) that for $\beta \ll 1$ and $\dot{\phi}(t) = \Delta f t / T$ the cost function for the ML estimator is approximately

$$C(t_0) = \beta \Re \left\{ e^{i\omega^2 T/(2\Delta f)} \left[\int \mathrm{d}t \left(i_1(t) - i_2(t) \right) e^{-i\omega t} \star A(\omega) \right] \right\} \Big|_{\omega = \Delta f t_0 / T}, \tag{26}$$

where $\star$ denotes convolution and $A(\omega) \equiv e^{-i\omega T/2} \sin(\omega T/2)/(\pi\omega)$ is the Fourier transform of the observation window $t \in (0, T]$. Thus, the cost function has an effective resolution width equal to $4\pi/\Delta f$. Dividing $\mathcal{T}$ into $n_{\mathrm{bin}} + 1$ bins with centers at $t_k = T_1 + k 4\pi/\Delta f$, for $k = 0, \ldots, n_{\mathrm{bin}}$, we approximate $P_{\mathcal{A}|2}$ by

$$P_{\mathcal{A}|2} = 1 - P\left(\bigcap_{\ell \neq k^*} C(t_{k^*}) > C(t_\ell) \right) \tag{27}$$

where k^* denotes the bin index that contains the true value t_0. In other words, a typical event occurs if the cost function is peaked at the bin encompassing the true t_0. A tractable expression for the right-hand side of this equation follows from assuming $C(t_k)$ are jointly Gaussian random variables. The mean of $C(t_k)$ is $\langle C(t_k)\rangle = (\eta N_I \beta^2/2)\delta_{k,k^*}$, and the covariance is given by $\mathrm{cov}(C(t_k), C(t_\ell)) = (\eta N_I \beta^2/2)\delta_{k,\ell}$, where δ is the Kronecker delta function. Consequently, via Eq. (27) we obtain

$$P_{\mathcal{A}|2} \approx 1 - \left[1 - Q\left(\sqrt{\eta N_I}\beta/2\right)\right]^{n_{\mathrm{bin}}}, \tag{28}$$

where $Q(x) \equiv \int_x^\infty \mathrm{d}t\, e^{-t^2/2}/\sqrt{2\pi}$. Substituting Eq. (28) back into Eq. (25) yields $P_{\mathcal{A}}$.

Having evaluated all of the components in Eq. (24), we can solve for N_ℓ. We perform several simplifying approximations to derive a tractable analytic expression. First, via Eq. (6) we use

$$\mathrm{CRB}^{-1} \approx \eta N_I \beta^2 \varepsilon_\phi, \tag{29}$$

where $\varepsilon_\phi \equiv T^{-1}\int_0^T \mathrm{d}t\, \dot{\phi}^2(t)$. Next, we use $(1-x)^n \approx 1 - nx$ for $nx \ll 1$ and $Q(x) \approx e^{-x^2/2}/2$ to obtain, via Eqs. (25) and (28),

$$P_{\mathcal{A}} \approx P_{\mathcal{A}|2} \approx \frac{n_{\mathrm{bin}}}{2} e^{-\eta N_I \beta^2/8}. \tag{30}$$

With the aid of these approximations we solve for the breakdown threshold as

$$N_\ell = -\frac{8}{\eta\beta^2} W_{-1}\left(\frac{-1}{4\varepsilon_\phi \sigma_{\mathcal{A}}^2 n_{\mathrm{bin}}}\right), \tag{31}$$

where $W_{-1}(y)$ is the Lambert-W function along the -1 branch, formally defined as the inverse of the function $y = xe^x$ for $x < -1$ [18].

In Figs. 4 and 5 we have plotted the N_ℓ predicted by Eq. (31), as well as the MSE model from Eq. (22) and the simulation-based MSE. In all three cases, the approximation to N_ℓ matches very well with the knee in the MSE model, indicating that it is a good analytic

approximation to the transition in the model. In comparing the model to the simulated MSE results we find that N_ℓ is higher than the breakdown threshold observed in simulation, but within a factor of three. Therefore, Eq. (31) offers a tractable approximation to the breakdown threshold that conservatively predicts the $N_I > N_\ell$ region in which the ML estimator may approach the standard quantum limit.

3.B. The upper breakdown threshold N_u

Dead time impairs the estimation performance when the average arrival rate of the incident photons significantly exceeds $1/\tau$, such that the detectors cannot respond to many information-carrying incident photons.

The impulse responses applied to $i_m(t)$ in the ML estimator—stated in Eq. (18)—indicate that the sufficient statistic in the presence of dead time is appreciably different from that when $\tau = 0$ if α is large enough to render the second term comparable to the first term. Suppose $x \equiv |\beta_d \cos\big(D(t;t_0)\big)| \in [0, \beta_d]$ in Eq. (18). The ratio of the first and second term amplitudes is smallest when $x = \beta_d$, so it is sufficient to consider this extreme point. Defining the precise ratio at which the threshold behavior manifests is heuristic in nature, but we choose

$$\log(1+\beta_d)/(\alpha\beta_d) = 1/2 \tag{32}$$

as a value that demonstrates consistent agreement with the simulated performance. Recognizing that $\beta_d \approx \beta$ and $\alpha \approx \eta N_I \tau/(2T)$ for $N_I \gg 1$, we arrive at the upper threshold value

$$N_u = \max\left\{\frac{\log(1+\beta)T}{\beta\tau}, N_\ell\right\}, \tag{33}$$

where the maximum is due to the fact that if the first term inside the brackets is less than N_ℓ then atypical events dominate the performance and the dead-time-induced blocking behavior is not visible until $N_I > N_\ell$.

The N_u we have defined above is plotted in the two simulations presented earlier in Fig. 5. In both cases it accurately predicts the regime in which dead time deteriorates the MSE of

the ML estimator. In Fig. 5(a) the three performance regimes are distinctly identifiable, and the MSE approaches the standard quantum limit only when $N_\ell < N_I < N_u$, as expected. In Fig. 5(b), on the other hand, we illustrate a $\beta \ll 1$ case when $N_\ell = N_u$, so the optimal $1/N_I$ scaling is never attainable. When the incident photon flux is sufficiently high to emerge from the regime in which atypical events dominate, it has already become too high for the dead time of the photodetectors. Consequently, the MSE transitions from the first breakdown regime directly into the dead-time-blocked regime, and never achieves shot-noise-limited performance.

In summary, the ML estimator can achieve the standard quantum limit with the optimal $1/N_I$ scaling of the MSE, provided that the total mean photon number incident on the two detectors satisfies

$$N_\ell < N_I < N_u, \tag{34}$$

where N_ℓ is given in Eq. (31) and N_u is given in Eq. (33). If we have $N_u = N_\ell$, then the standard quantum limit is not attainable.

4. Experimental Results

We have performed a proof-of-concept FMCW ranging experiment using linear frequency modulation and photon-counting Geiger-mode avalanche photodiodes (APDs). Here we report on the performance of the ML estimator and discuss insights gained from this experiment.

Figure 6 provides a block diagram of the experimental setup. A linear sawtooth frequency modulation with rate 33.3 GHz/ms and period 1.25 ms is applied to a 1539 nm center-wavelength distributed feedback laser, using active phase locking. 10% of the output power is used in this feedback loop. Furthermore, only the central linearized portion of each period is used in collecting the experimental data, to avoid transients that occur around the sharp frequency transitions. The remaining output power (90%) passes through several attenuators, including a variable attenuator for power adjustment, and 99/1 splitters for power monitor-

ing. An in-line polarizer is used to maintain polarization. This source field is then split into the signal and reference arms via a 50/50 splitter. The signal field passes through a circulator and then is sent out to the target mirror, which is placed approximately 0.8 m away on the optical bench. The return field is recoupled into the circulator and is recombined with the reference field on a 50/50 splitter. The resulting beat frequency is approximately 40 kHz, indicating a relative path length of approximately 18 cm. The outputs of the beamsplitter are incident on two matched Geiger-mode photon-counting APDs, which have quantum efficiency of 0.1, dark noise level 1000 counts/s, and dead time 1 μs. The output photoelectrons in each detector are time-tagged via a time-to-digital converter (TDC) unit over a period of 990 μs. The reference arm path includes a short delay line for fine adjustments to the beat frequency, and an in-line polarizer to maintain polarization.

The experiment was run at 21 flux levels spanning approximately from 10 to 30000 mean incident photons per period,[6] and at each flux rate 8000 independent data sets were collected. Two estimators were applied to each set: the ML estimator, and an estimator that performs difference detection followed by evaluating the square-magnitude of the Fourier transform and peak identification. For convenience, hereon we refer to the latter as the Fast Fourier Transform (FFT) estimator. In order to achieve good performance it was necessary to make a small modification to the ML estimator in Eq. (16). The sharp transitions at the end of each period in the sawtooth modulation triggers reacquisition of the feedback loop, which results in an unknown initial acquisition frequency in each period. Thus, the linear frequency modulation function of the ML estimator was modified as $\dot{\phi}(t) = \Delta f(t - t_i)/T$, and t_i and t_0 were estimated jointly.

At each power level the square error in the 8000 estimates were averaged to calculate a mean-square error. A fair assessment of the estimator performance requires an accurate knowledge of the true range to the target. A calibration run with high photon flux (yielding approximately 1368 counts per integration window) was performed, and the ML estimate

[6]The incident photon number is estimated for $\alpha \ll 1$ by setting $\eta N_I(1 + \alpha(1 - \beta^2/2))/(1 + 2\alpha)$ equal to the mean photoelectron counts and solving for ηN_I, which accounts for the counts lost to dead time.

at that photon flux was assumed as the true range to the target.[7] Figure 7 shows the experimental root-mean-square error obtained with the ML estimator and the FFT estimator, as a function of ηN_I. The CRB and the analytic error model for the ML estimator are also plotted for comparison. Both estimators demonstrate good agreement with the breakdown threshold predicted by the theoretical model, although the ML estimator demonstrates a transient gap to the CRB before it asymptotically converges with the CRB as expected. We conjecture that this is due to the acquisition frequency ambiguity discussed earlier. The FFT estimator on the other hand demonstrates a factor of 3.8 penalty relative to the CRB, and a factor of 3.4 relative to the ML estimator performance.

5. Discussion

In this paper we have provided detailed analysis of optimal range estimation using frequency-modulated ideal laser light and continuous-time photon counting detectors that output time-tagged photon arrivals. Our analysis has centered around three themes: understanding the best possible performance via a study of the CRB, characterizing the performance of the ML estimator, and experimentally validating the theory with a proof-of-concept experiment. The theory that we have developed is sufficiently broad to provide a unified treatment of some of the important recent advances in employing different frequency modulations, as well as varying signal and reference field strengths. It can also be applied to other optical remote sensing instruments where frequency estimates are calculated from coherently-detected fields, e.g., coherent Doppler lidar.

Our CRB results reveal that the best-case mean-square error scales as $1/N_I$. Furthermore, if the signal and reference field photons have equal cost, the optimal strength of the reference field is equal to the field strength of the target-return field. When this condition is met, the primary feature of the frequency modulation that impacts the CRB is its average energy,

[7] It is best to obtain the target range truth via an independent measurement. However, this was not practical to perform on our bench-top experiment configuration. Thus, we have opted to use the mean value of the ML and FFT estimators at the highest photon flux as the true distance to the target.

which has permitted us to quantify the gains from employing different modulations. When photodetector dark counts and dead time are included the CRB admits to three distinct regimes: 1) if dark counts dominate over signal counts the CRB scales as N_d/N_I^2; 2) if the signal counts are high enough to dominate over dark counts but are not so high that dead time blocks the detectors, the standard quantum limit prevails; and 3) if dead time blocks observation of most incident photon arrivals the CRB is constant with N_I. Simulating the ML estimator has revealed two thresholds, N_ℓ and N_u, such that when $N_\ell < N_I < N_u$ the performance is approximately equal to the standard quantum limit, but otherwise the performance is bounded away from this optimal scaling. We have derived analytic approximations to these thresholds when linear frequency modulation is used, which identifies the optimal performance regime in terms of critical system parameters. Finally, we have performed an experimental proof-of-concept with equal reference and target-return field strengths, demonstrating that the ML estimator behaves as predicted and that it outperforms conventional frequency-domain estimation.

While the ML estimator has many desirable optimality properties, it also has some shortcomings that should be addressed. First, the ML estimator must know β, which implies that the mean photon number in the target-return arm must be estimated. In this paper we have assumed that β has been measured and is available to the estimator. However, in scenarios when this is not feasible β and t_0 must be estimated jointly, which may increase estimation time and implementation complexity. Second, the ML estimator utilizes information in the phase of the rate functions, in addition to that in the beat frequency. Therefore it is more sensitive to auxiliary parameters than the conventional frequency-domain estimator we have introduced in Section 4 (the FFT estimator). Simplifications to the ML estimator are often sought to speed-up computation time, reduce complexity, or improve robustness at the expense of some loss in performance. Although here we have not addressed these trades, the FFT estimator does emerge as a good candidate for linear frequency modulation.

In a field-deployed ranging system several additional uncertainties resulting from the en-

vironment are significant. In particular, in this paper we have not considered the effects of rough-surface scattering off of the target, atmospheric turbulence induced amplitude and phase fluctuations in the target-return signal, ambient background radiation, photodetector timing jitter, and calibration errors. The theory presented in this paper could be, in principle, extended to encompass these effects by deriving the proper joint probability density function of the photon-arrival times. However, this may prove too complex for tractable and insightful analytic results.

In summary, we have provided a rigorous and detailed analysis of FMCW ranging with ideal laser fields and photon-counting detectors. We have derived the CRB, including the impact of dark counts and dead time. We have shown that the ML estimator can attain the optimal CRB scaling of $1/N_I$ if the mean received photon number satisfies $N_\ell < N_I < N_u$. We have verified the performance of the ML estimator via a proof-of-concept experiment and shown that it performs better than the conventional FFT estimator.

A. Appendix: Derivation of Cramér-Rao bound and ML estimator

We derive the CRB and the ML estimator for general dark count rate and dead time. Setting these parameters to zero yields the near-ideal results in Section 2. Consider a pair of matched photon-counting detectors in the Fig. 1 setup, having quantum efficiency η, mean dark rate λ_d (in photoelectrons/s) and dead time τ (in seconds). In the following derivation we will use $\Lambda_{m,d}(t) \equiv \Lambda_{m,d}(t; t_0)$ to keep our notation compact.

The CRB is defined in Eq. (5) and the probability density function for the photoelectron counts is given in Eqs. (10)–(11). Taking the logarithm in Eq. (10) yields

$$\log p(n_1, u_1, \ldots, u_{n_1}, n_2, v_1, \ldots, v_{n_2}; t_0) = \sum_{m=1}^{2} \log f(n_m, u_1, \ldots, u_{n_m}; t_0) + C_1 \qquad (35)$$

where $C_1 \equiv \int_0^T \mathrm{d}t\,[\Lambda_{1,d}(t) + \Lambda_{2,d}(t)]$ is a constant independent of t_0, and

$$f(n_m, u_1, \ldots, u_{n_m}; t_0) \equiv \sum_{i=1}^{n_m} \log\big(\Lambda_{m,d}(u_i)\big) + \sum_{i=2}^{n_m+1} \int_{u_{i-1}}^{u_i} \mathrm{d}t\,\Lambda_{m,d}(t)\big(1 - w_\tau(t - u_{i-1})\big) \tag{36}$$

for $m = 1, 2$. We may express Eq. (36) as

$$f(n_m, u_1, \ldots, u_{n_m}; t_0) \equiv \int_0^T \mathrm{d}t\,i_m(t)\big(\log \Lambda_{m,d}(t) + L_m(t)\big) + \int_{u_{n_m}+\tau}^T \mathrm{d}t\,\Lambda_m(t), \tag{37}$$

in terms of $L_m(t) \equiv \int_t^{t+\tau} \mathrm{d}t\,\Lambda_{m,d}(t)$. We ignore the last term because it is an edge effect that is typically small. In the limit that the rate functions $\Lambda_{m,d}(t)$ vary slowly over the duration τ, i.e., when $|\mathrm{d}D(t;t_0)/\mathrm{d}t|\tau \ll 1$, we have $L_m(t) \approx \tau\Lambda_{m,d}(t)$, yielding

$$f(n_m, u_1, \ldots, u_{n_m}; t_0) \approx \int_0^T \mathrm{d}t\,i_m(t)\big(\log \Lambda_{m,d}(t) + \tau\Lambda_{m,d}(t)\big). \tag{38}$$

Substituting Eq. (38) into Eq. (35), and that into Eq. (5) yields

$$\mathrm{CRB}^{-1} = \sum_{m=1}^{2} \int_0^T \mathrm{d}t\,\langle i_m(t)\rangle \left[\frac{\dot{\Lambda}_{m,d}^2(t)}{\Lambda_{m,d}^2(t)} - \frac{\ddot{\Lambda}_{m,d}(t)}{\Lambda_{m,d}(t)} - \tau\ddot{\Lambda}_{m,d}(t)\right]. \tag{39}$$

where we have used the shorthand notation $\dot{\Lambda}_{m,d}(t) \equiv \mathrm{d}\Lambda_{m,d}(t)/\mathrm{d}t_0$ and $\ddot{\Lambda}_{m,d}(t) \equiv \mathrm{d}^2\Lambda_{m,d}(t)/\mathrm{d}t_0^2$.

The last step of evaluating the CRB is to find $\langle i_m(t)\rangle$. In general, this expectation is difficult to derive for self-exciting stochastic processes. However, when the rate function varies slowly relative to the dead time interval such that $L_m(t) \approx \tau\Lambda_{m,d}(t)$ holds, it has been shown that the average photocurrent is expressible as [19]

$$\langle i_m(t)\rangle = \frac{\Lambda_{m,d}(t)}{1 + \tau\Lambda_{m,d}(t)}. \tag{40}$$

This mean arrival rate has intuitive asymptotes. When $\Lambda_{m,d}(t) \ll 1$, we have $\langle i_m(t)\rangle \approx$

$\Lambda_{m,d}(t)$, indicating that the impact of dead time is negligible. On the other hand, if $\Lambda_{m,d}(t) \gg 1$, the detector is continually blocked by arrivals occurring every τ seconds, so the mean arrival rate converges to $\langle i_m(t) \rangle \approx 1/\tau$.

Substituting Eq. (40) into (39), recognizing that $\dot{\Lambda}_1(t) = -\dot{\Lambda}_2(t)$ and $\ddot{\Lambda}_1(t) = -\ddot{\Lambda}_2(t)$, and some straightforward algebraic manipulation results in

$$\mathrm{CRB}^{-1} = \int_0^T \mathrm{d}t \, \dot{\Lambda}_{1,d}^2(t) \left[\sum_{m=1}^{2} \frac{1}{\Lambda_{m,d}(t)\big(1 + \tau \Lambda_{m,d}(t)\big)} \right]. \tag{41}$$

Finally, substituting the Eq. (9) rate functions into this expression, we arrive at

$$\mathrm{CRB} = \frac{1}{\eta N_{I,d}} \left[\frac{1}{T} \int_0^T \mathrm{d}t \, \frac{\beta_d^2 \sin^2\big(D(t;t_0)\big)}{1 - \beta_d^2 \cos^2\big(D(t;t_0)\big)} \dot{\phi}^2(t - t_0) \frac{1 + \alpha\big[1 + \beta_d^2 \cos^2\big(D(t;t_0)\big)\big]}{1 + 2\alpha + \alpha^2\big[1 - \beta_d^2 \cos^2\big(D(t;t_0)\big)\big]} \right]^{-1}, \tag{42}$$

where $\alpha = \eta N_{I,d} \tau / (2T)$. The Eq. (12) asymptotes follow from considering the corresponding limits of this expression. To obtain the standard quantum limit stated in Eq. (6) we set $N_d = 0$ and $\alpha = 0$.

To derive the ML estimator we start with the logarithm of the probability density function that we have derived above. Substituting Eqs. (35) and (38) into Eq. (16), followed by some straightforward simplifications of the expressions, yields the linear filtering form of Eq. (17) with the impulse responses specified in Eq. (18).

Acknowledgments

BIE's contributions to the research described in this paper was supported by the DARPA InPho program under contract number PROP. 81-17433, and was carried out by the Jet Propulsion Laboratory, California Institute of Technology, under a contract with the National Aeronautics and Space Administration. ZWB's and JD's contributions were supported by the DARPA InPho program, under Army Research Office Grant W911NF-11-1-0540.

References

1. M.-C. Amann, T. Bosch, M. Lescure, R. Myllylä, and M. Rioux, "Laser ranging: a critical review of usual techniques for distance measurement," Opt. Eng. **40**, 10–19 (2001).
2. H. L. V. Trees, *Detection, Estimation and Modulation Theory, Part 1* (Prentice Hall, New York, 2001).
3. N. Satyan, A. Vasilyev, G. Rakuljic, V. Leyva, and A. Yariv, "Precise control of broadband frequency chirps using optoelectronic feedback," Opt. Express **17**, 15991–15999 (2009).
4. Z. W. Barber, W. R. Babbitt, B. Kaylor, R. R. Reibel, and P. A. Roos, "Accuracy of active chirp linearization for broadband frequency modulated continuous-wave ladar," Appl. Opt. **49**, 213–219 (2010).
5. L. T. Masters, M. B. Mark, and B. D. Duncan, "Analysis of ladar range resolution enhancement by sinusoidal phase modulation," Opt. Eng. **34**, 3115–3121 (1995).
6. D. Dupuy, M. Lescure, and M. Cousineau, "A FMCW laser range-finder based on a delay line technique," Proc. IEEE Instrum. Meas. Tech. Conf. **2**, 1084–1088 (2001).
7. K. Asaka, Y. Hirano, K. Tatsumi, K. Kasahara, and T. Tajime, "A pseudo-random frequency modulation continuous wave coherent lidar using an optical field correlation detection method," Opt. Rev. **5**, 310–314 (1998).
8. L. A. Jiang and J. X. Luu, "Heterodyne detection with a weak local oscillator," Appl. Opt. **47**, 1486–1503 (2008).
9. T. J. Green and J. H. Shapiro, "Maximum-likelihood laser radar range profiling with the expectation-maximization algorithm," Opt. Eng. **31**, 2343–2354 (1992).
10. S. Hernandez-Marin, A. M. Wallace, and G. J. Gibson, "Bayesian analysis of lidar signals with multiple returns," IEEE Trans. Pattern Anal. Mach. Intell. **29**, 2170–2180 (2007).
11. T. J. Karr, "Atmospheric phase error in coherent laser radar," IEEE Trans. Antennas Propag. **55**, 1122–1133 (2007).
12. L. Mandel and E. Wolf, *Optical Coherence and Quantum Optics* (Cambridge Univ.,

Cambridge, 1995).

13. R. M. Gagliardi and S. Karp, *Optical Communications* (Wiley, New York, 1976).
14. D. L. Snyder, *Random Point Processes* (Wiley, New York, 1975).
15. P. Forster, P. Larzabal, and E. Boyer, "Threshold performance analysis of maximum likelihood DOA estimation," IEEE Trans. Signal Process. **52**, 3183–3191 (2004).
16. F. Athley, "Threshold region performance of maximum likelihood direction of arrival estimators," IEEE Trans. Signal Process. **53**, 1359–1373 (2005).
17. B. I. Erkmen and B. Moision, "Maximum likelihood time-of-arrival estimation of optical pulses via photon-counting photodetectors," Proc. 2009 IEEE ISIT, 1909–1913 (2009).
18. R. M. Corless, G. H. Gonnet, D. E. G. Hare, D. J. Jeffrey, and D. E. Knuth, "On the Lambert W function," Adv. Comput. Math. **5**, 329–359 (1996).
19. G. Vannucci and M. C. Teich, "Effects of rate variation on the counting statistics of dead-time-modified Poisson processes," Opt. Commun. **25**, 267–272 (1978).

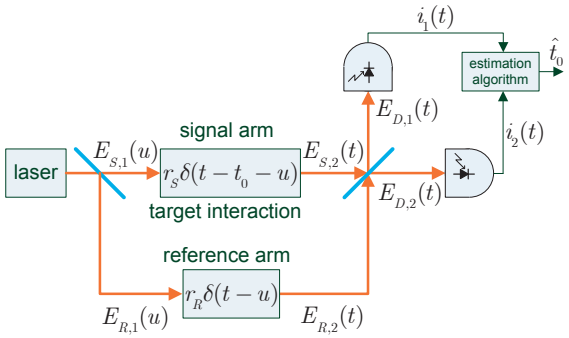

Fig. 1. Block diagram of FMCW ranging. Optical fields are denoted with thick (orange) lines and electrical signals are denoted with thin (black) lines.

Type	$\dot{\phi}(t)$, $0 < t \leq T$	$T^{-1} \int_0^T \mathrm{d}t\, \dot{\phi}^2(t)$
linear	$\Delta f t/T$	$(\Delta f)^2/3$
polynomial	$\Delta f (t/T)^p$, $p > 0$	$(\Delta f)^2/(2p+1)$
sinusoid	$\Delta f \sin(2\pi t/T)$	$(\Delta f)^2/2$
(pseudo) random	$\Delta f \sum_{k=1}^K a_k b_k(t)$, $a_k \in \{-1, 1\}$	$(\Delta f)^2$

Table 1. $\mathcal{L}_2$ norms of various frequency modulations with identical peak-to-peak frequency variation Δf. In the last entry, $b_k(t) \equiv 1$ for $2K|t - (k - 1/2)T/K|/T < 1$ and 0 otherwise.

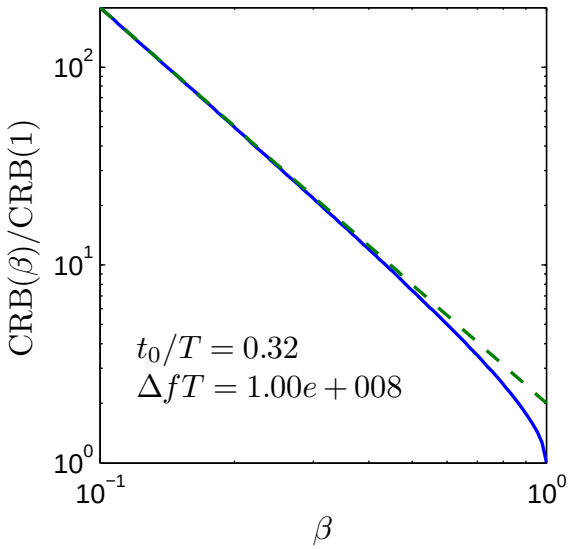

Fig. 2. The ratio of the CRB for $\beta < 1$ to that at $\beta = 1$. The solid (blue) curve is obtained by numerically evaluating the exact expression, whereas the dashed (green) line corresponds to the $\beta \ll 1$ approximation to the CRB.

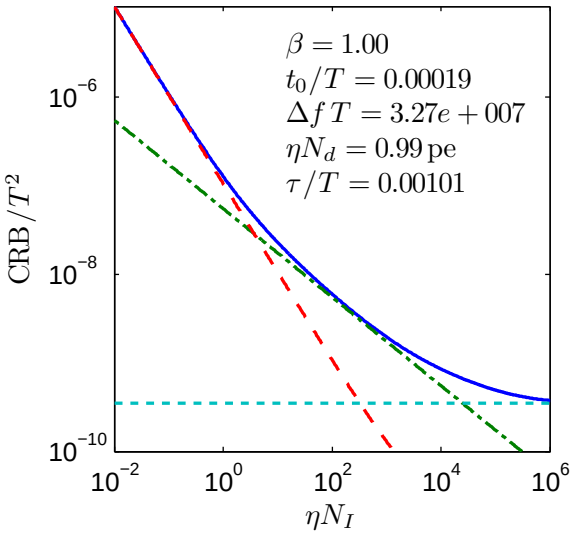

Fig. 3. The exact CRB, normalized by T^2, is shown as the solid (blue) line. The dashed (red) line is the dark noise asymptote, the dash-dotted (green) line indicates the shot noise asymptote, and the dotted (cyan) line is the dead time asymptote.

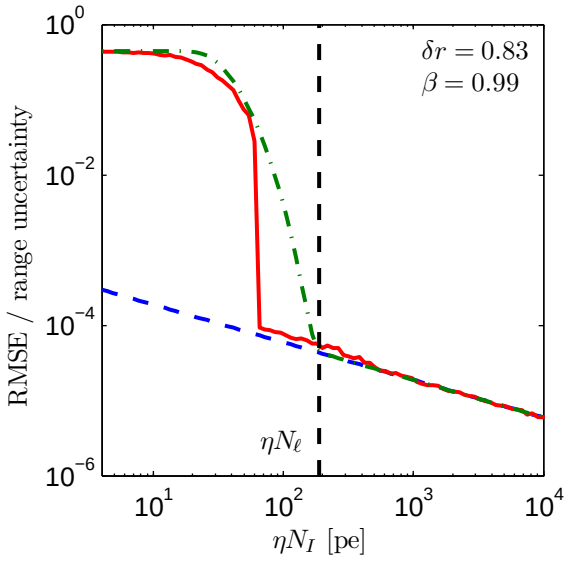

Fig. 4. A plot of the root-mean-square error (RMSE) normalized to the width of the range uncertainty window. The solid (red) line is the simulated performance of the ML estimator, the dashed (blue) line is the CRB, and the dash-dotted (green) line is the analytic MSE model. The vertical dashed line is ηN_ℓ. δr is the fractional position of the object in its support.

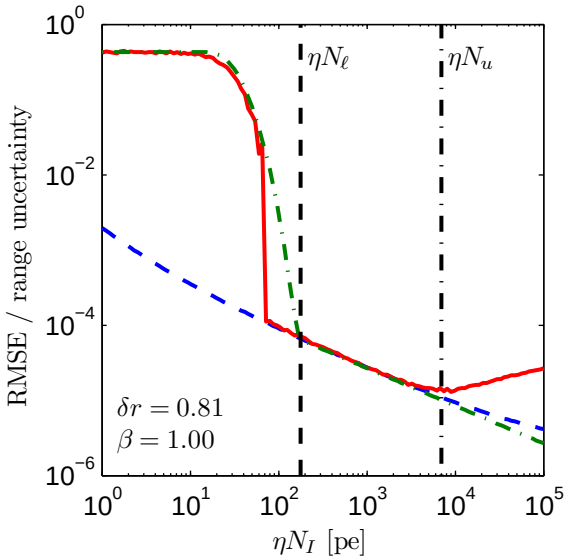

(a)

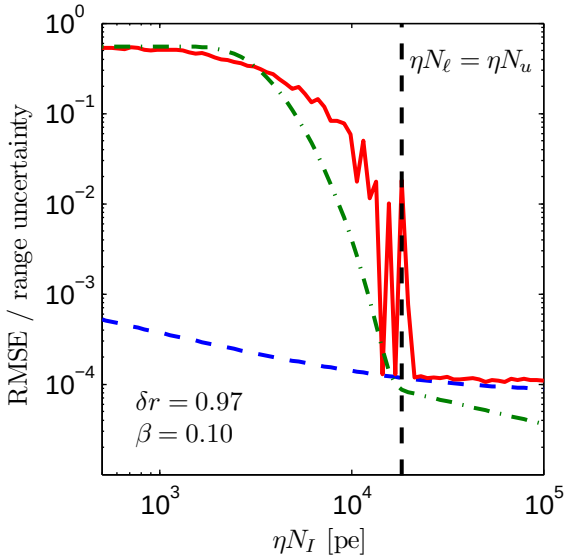

(b)

Fig. 5. A plot of the root-mean-square error (RMSE) normalized to the width of the range uncertainty window. The solid (red) line is the simulated performance of the ML estimator, the dashed (blue) line is the CRB, and the dash-dotted (green) line is the analytic MSE model. Vertical lines correspond to predicted thresholds. δr is the fractional position of the object in its support.

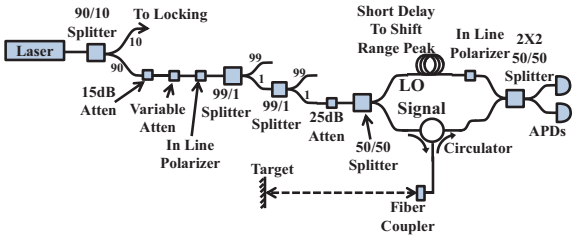

Fig. 6. Block diagram of FMCW ranging experiment.

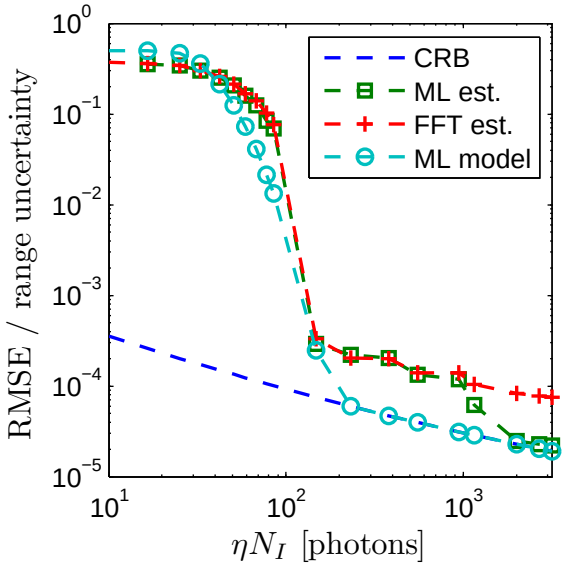

Fig. 7. Performance of the ML estimator and the FFT estimator, plotted as a function of ηN_I. The CRB and the ML error model are plotted for comparison.